Supplement to: A Novel Interpretable Fusion Analytic Framework for Investigating Functional Brain Connectivity Differences in Cognitive Impairments

Jeong-Jae Kim[1,*], Yeseul Jeon[2,*], SuMin Yu[3], Junggu Choi[1], and Sanghoon Han[1,4,+]

[1]Graduate Program in Cognitive Science, Yonsei University, Seoul, Republic of Korea
[2]Department of Statistics and Data Science, Yonsei University, Seoul, Republic of Korea
[3]Department of Psychology and Neuroscience, Duke University, Durham, North Carolina, USA
[4]Department of Psychology, Yonsei University, Seoul, Republic of Korea
[*]These authors contributed equally to this work
[+]Corresponding author : sanghoon.han@yonsei.ac.kr

ABSTRACT

Functional magnetic resonance imaging (fMRI) data is characterized by its complexity and high–dimensionality, encompassing signals from various regions of interests (ROIs) that exhibit intricate correlations. Analyzing fMRI data directly proves challenging due to its intricate structure. Nevertheless, ROIs convey crucial information about brain activities through their connections, offering insights into distinctive brain activity characteristics between different groups. To address this, we propose a cutting-edge interpretable fusion analytic framework that facilitates the identification and understanding of ROI connectivity disparities between two groups, thereby revealing their unique features. Our novel approach encompasses three key steps. Firstly, we construct ROI functional connectivity networks (FCNs) to effectively manage fMRI data. Secondly, employing the FCNs, we utilize a self–attention deep learning model for binary classification, generating an attention distribution that encodes group differences. Lastly, we employ a latent space item-response model to extract group representative ROI features, visualizing these features on the group summary FCNs. We validate the effectiveness of our framework by analyzing four types of cognitive impairments, showcasing its capability to identify significant ROIs contributing to the differences between the two disease groups. This novel interpretable fusion analytic framework holds immense potential for advancing our understanding of cognitive impairments and could pave the way for more targeted therapeutic interventions.

Supplementary Figures and Tables

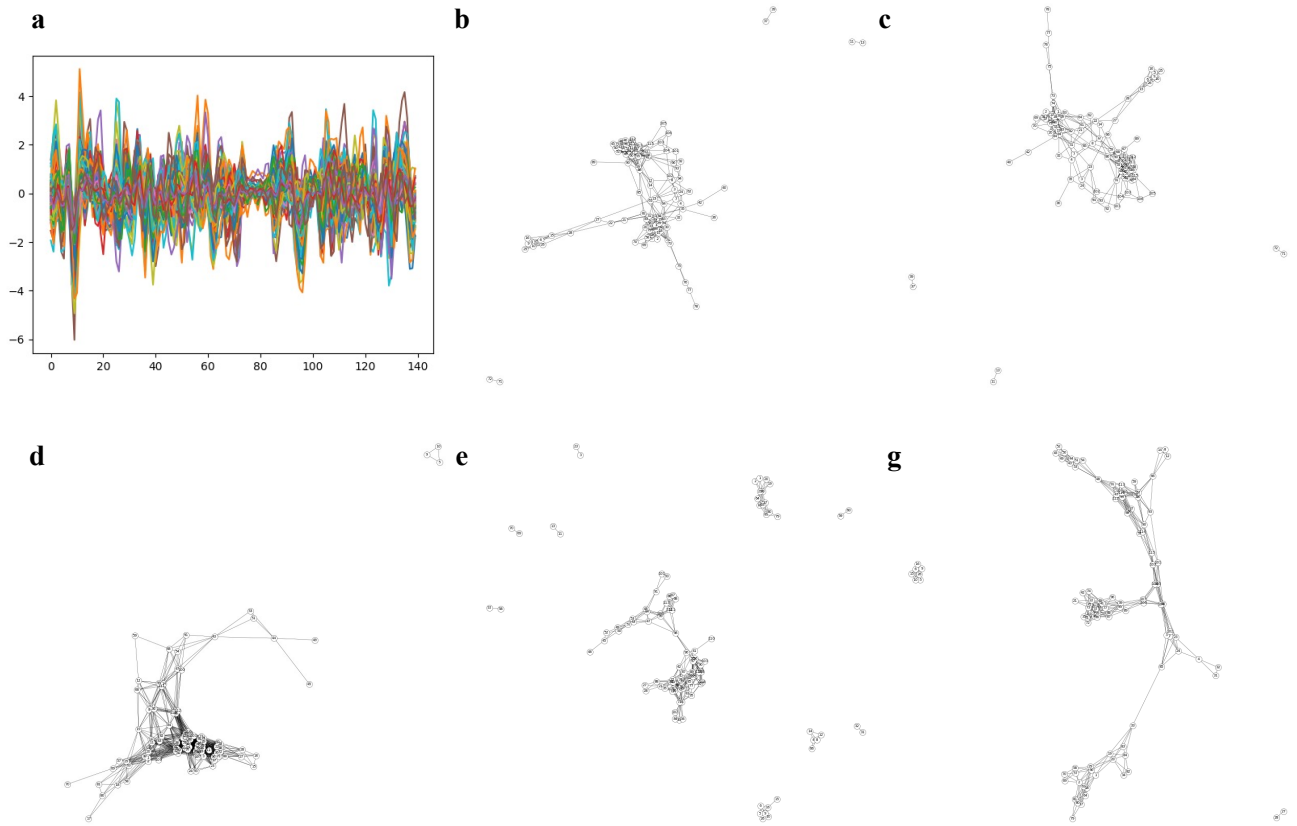

Supplementary Figure 1. Correlation coefficient based FCNs and dimension reduction based FCNs of MCI subject. (**a**) illustrates the ROIs, rs-fMRI BOLD signals for a sample of subjects with MCI. These FCN graphs were generated using various approaches. Firstly, we employed correlation-based methods such as Pearson's r or Fisher's z values (shown in (**b**) and (**c**) to establish intricate and interconnected FCNs. However, comprehending the specific attributes of each brain region within these correlation-based FCNs proved challenging. To gain a deeper understanding of the interrelationships between brain regions, we employed dimension reduction techniques to estimate the latent positions of the brain regions. (**d**) demonstrates the brain region patterns embedded in a 2D space with the highest exploratory power, obtained through PCA in linear space. Additionally, we utilized t-SNE (stochastic space-based FCN) as shown in (**e**), which assumes that the patterns between brain regions follow a specific probability distribution and learns the degree of similarity between these distributions. Furthermore, we employed UMAP (topological space-based FCN) depicted in (**f**) to capture the topological similarity of the waveform patterns generated by the ROIs.

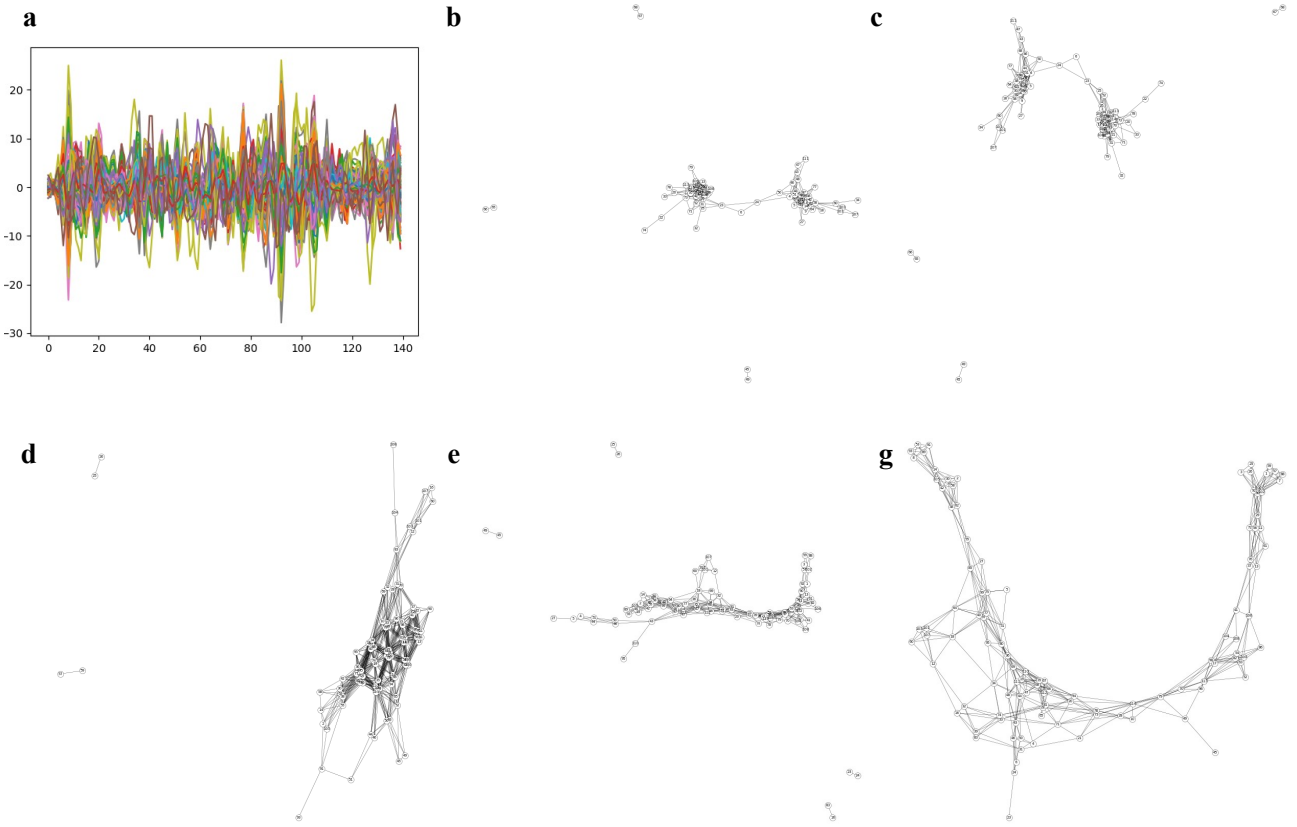

Supplementary Figure 2. Correlation coefficient based FCNs and dimension reduction based FCNs of EMCI subject. (**a**) illustrates the ROIs, rs-fMRI BOLD signals for a sample of subjects with EMCI. These FCN graphs were generated using various approaches. Firstly, we employed correlation-based methods such as Pearson's r or Fisher's z values (shown in (**b**) and (**c**) to establish intricate and interconnected FCNs. However, comprehending the specific attributes of each brain region within these correlation-based FCNs proved challenging. To gain a deeper understanding of the interrelationships between brain regions, we employed dimension reduction techniques to estimate the latent positions of the brain regions. (**d**) demonstrates the brain region patterns embedded in a 2D space with the highest exploratory power, obtained through PCA in linear space. Additionally, we utilized t-SNE (stochastic space-based FCN) as shown in (**e**), which assumes that the patterns between brain regions follow a specific probability distribution and learns the degree of similarity between these distributions. Furthermore, we employed UMAP (topological space-based FCN) depicted in (**f**) to capture the topological similarity of the waveform patterns generated by the ROIs.

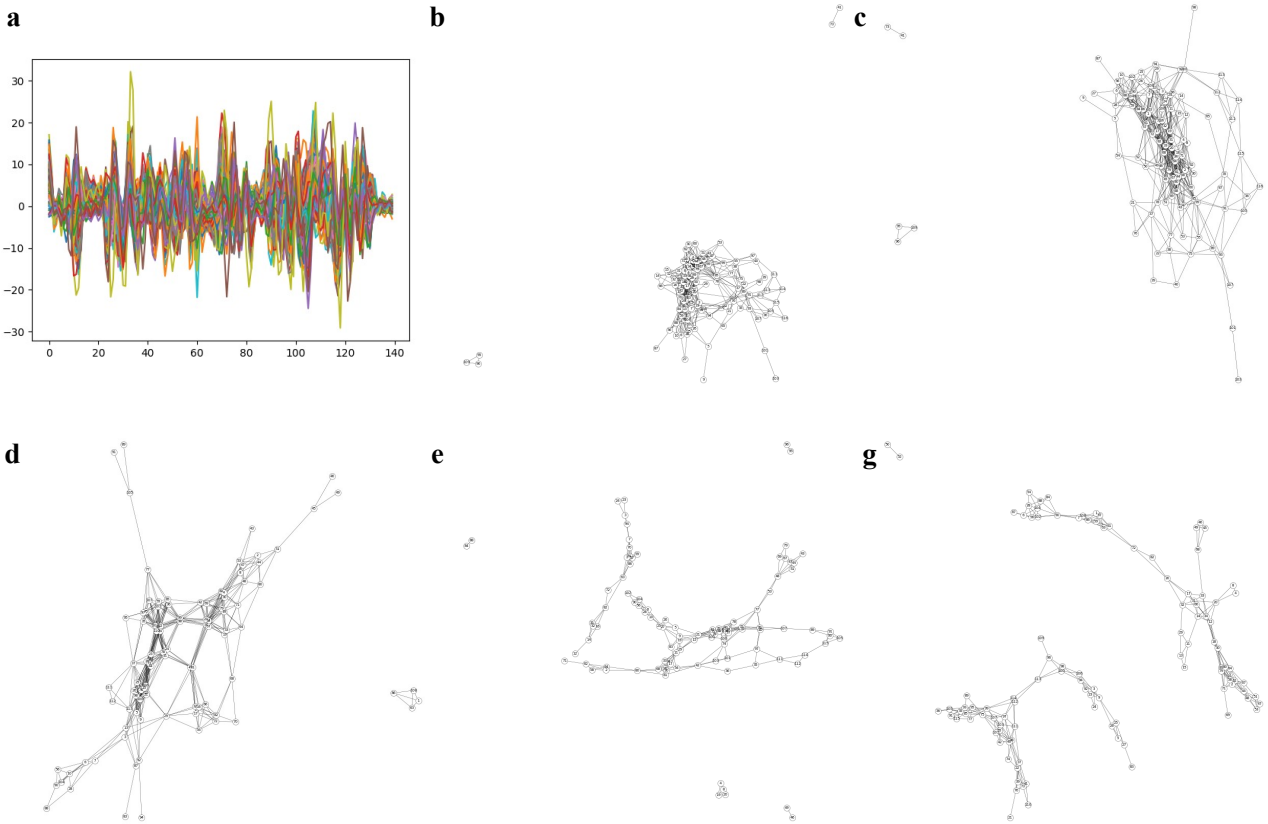

Supplementary Figure 3. Correlation coefficient based FCNs and dimension reduction based FCNs of LMCI subject. (**a**) illustrates the ROIs, rs-fMRI BOLD signals for a sample of subjects with LMCI. These FCN graphs were generated using various approaches. Firstly, we employed correlation-based methods such as Pearson's r or Fisher's z values (shown in (**b**) and (**c**) to establish intricate and interconnected FCNs. However, comprehending the specific attributes of each brain region within these correlation-based FCNs proved challenging. To gain a deeper understanding of the interrelationships between brain regions, we employed dimension reduction techniques to estimate the latent positions of the brain regions. (**d**) demonstrates the brain region patterns embedded in a 2D space with the highest exploratory power, obtained through PCA in linear space. Additionally, we utilized t-SNE (stochastic space-based FCN) as shown in (**e**), which assumes that the patterns between brain regions follow a specific probability distribution and learns the degree of similarity between these distributions. Furthermore, we employed UMAP (topological space-based FCN) depicted in (**f**) to capture the topological similarity of the waveform patterns generated by the ROIs.

#	Name	#	Name	#	Name	#	Name
1	Precentral_L	30	Insula_R	59	Parietal_Sup_L	88	Temp_Pole_Mid_R
2	Precentral_R	31	Cingulum_Ant_L	60	Parietal_Sup_R	89	Temporal_Inf_L
3	Frontal_Sup_L	32	Cingulum_Ant_R	61	Parietal_Inf_L	90	Temporal_Inf_R
4	Frontal_Sup_R	33	Cingulum_Mid_L	62	Parietal_Inf_R	91	Cerebelm_Crus1_L
5	Frontal_Sup_Orb_L	34	Cingulum_Mid_R	63	SupraMarginal_L	92	Cerebelm_Crus1_R
6	Frontal_Sup_Orb_R	35	Cingulum_Post_L	64	SupraMarginal_R	93	Cerebelm_Crus2_L
7	Frontal_Mid_L	36	Cingulum_Post_R	65	Angular_L	94	Cerebelm_Crus2_R
8	Frontal_Mid_R	37	Hippocampus_L	66	Angular_R	95	Cerebelum_3_L
9	Frontal_Mid_Orb_L	38	Hippocampus_R	67	Precuneus_L	96	Cerebelum_3_R
10	Frontal_Mid_Orb_R	39	ParaHippo_L	68	Precuneus_R	97	Cerebelum_4_5_L
11	Frontal_Inf_Oper_L	40	ParaHippo_R	69	Paracentral_Lob_L	98	Cerebelum_4_5_R
12	Frontal_Inf_Oper_R	41	Amygdala_L	70	Paracentral_Lob_R	99	Cerebelum_6_L
13	Frontal_Inf_Tri_L	42	Amygdala_R	71	Caudate_L	100	Cerebelum_6_R
14	Frontal_Inf_Tri_R	43	Calcarine_L	72	Caudate_R	101	Cerebelum_7_L
15	Frontal_Inf_Orb_L	44	Calcarine_R	73	Putamen_L	102	Cerebelum_7_R
16	Frontal_Inf_Orb_R	45	Cuneus_L	74	Putamen_R	103	Cerebelum_8_L
17	Rolandic_Oper_L	46	Cuneus_R	75	Pallidum_L	104	Cerebelum_8_R
18	Rolandic_Oper_R	47	Lingual_L	76	Pallidum_R	105	Cerebelum_9_L
19	Supp_Motor_L	48	Lingual_R	77	Thalamus_L	106	Cerebelum_9_R
20	Supp_Motor_R	49	Occipital_Sup_L	78	Thalamus_R	107	Cerebelum_10_L
21	Olfactory_L	50	Occipical_Sup_R	79	Heschl_L	108	Cerebelum_10_R
22	Olfactory_R	51	Occipital_Mid_L	80	Heschl_R	109	Vermis_1_2
23	Frontal_Sup_Med_L	52	Occipical_Mid_R	81	Temporal_Sup_L	110	Vermis_3
24	Frontal_Sup_Med_R	53	Occipital_Inf_L	82	Temporal_Sup_R	111	Vermis_4_5
25	Frontal_Mid_Orb_L	54	Occipital_Inf_R	83	Templ_Pole_Sup_L	112	Vermis_6
26	Frontal_Mid_Orb_R	55	Fusiform_L	84	Templ_Pole_Sup_R	113	Vermis_7
27	Rectus_L	56	Fusiform_R	85	Temporal_Mid_L	114	Vermis_8
28	Rectus_R	57	Postcentral_L	86	Temporal_Mid_R	115	Vermis_9
29	Insula_L	58	Postcentral_R	87	Templ_Pole_Mid_L	116	Vermis_10

Supplementary Table 1. Automated anatomical labeling–116 template

Top	AD vs MCI		AD vs EMCI	
	AD	MCI	AD	EMCI
Top–1	Postcentral_L	Cingulum_Mid_L	Fusiform_R	Fusiform_L
Top–2	Postcentral_R	Postcentral_L	Cerebelum_6_L	Temporal_Inf_L
Top–3	Temporal_Inf_L	Fusiform_R	Pallidum_R	Cingulum_Mid_L
Top–4	Supp_Motor_Area_R	Precentral_R	Postcentral_L	Pallidum_R
Top–5	Fusiform_L	Pallidum_L	Fusiform_L	Fusiform_R
Top–6	Cingulum_Mid_L	Temporal_Inf_L	Cerebelum_6_R	Frontal_Inf_Orb_L
Top–7	Fusiform_R	Fusiform_L	Hippocampus_R	Cerebelum_6_L
Top–8	Cerebelum_8_R	Supp_Motor_Area_R	Cingulum_Mid_L	Frontal_Inf_Tri_R
Top–9	Cerebelum_6_L	Insula_L	Cerebelum_7b_L	Putamen_R
Top–10	Putamen_L	Cerebelum_6_R	Putamen_R	Cingulum_Mid_R
Top–11	Cerebelum_8_L	Cerebelum_4_5_R	Cerebelum_4_5_L	Cerebelum_6_R
Top–12	Precentral_R	Postcentral_R	Temporal_Inf_L	Temporal_Inf_R
Top–13	Thalamus_L	Cerebelum_4_5_L	Cingulum_Mid_R	Vermis_8
Top–14	Temporal_Mid_R	Cerebelum_6_L	Cerebelum_8_L	Insula_L
Top–15	Cerebelum_4_5_R	Putamen_R	Hippocampus_L	Pallidum_L
Top–16	Insula_R	Cerebelum_8_R	Rolandic_Oper_R	Frontal_Sup_R
Top–17	Rolandic_Oper_R	Cerebelum_Crus2_R	Pallidum_L	Cerebelum_9_R
Top–18	Precentral_L	SupraMarginal_R	Cerebelum_Crus2_L	Temporal_Sup_R
Top–19	Temporal_Inf_R	Rolandic_Oper_R	Cerebelum_7b_R	Postcentral_L
Top–20	Insula_L	Hippocampus_R	Putamen_L	Cerebelum_7b_L
Top–21	Putamen_R	Cingulum_Mid_R	Temporal_Inf_R	Cerebelum_8_R
Top–22	Cerebelum_7b_R	Pallidum_R	Insula_L	Rolandic_Oper_L
Top–23	Temporal_Mid_L	Thalamus_L	Cerebelum_Crus2_R	Putamen_L
Top–24	Hippocampus_R	Putamen_L	Rolandic_Oper_L	Rolandic_Oper_R
Top–25	Cerebelum_4_5_L	Vermis_4_5	Cerebelum_8_R	Insula_R
Top–26	Cerebelum_10_R	Paracentral_Lobule_L	Cerebelum_3_L	Cerebelum_Crus2_L
Top–27	Cingulum_Mid_R	Vermis_8	Frontal_Inf_Tri_R	Cerebelum_3_L
Top–28	Pallidum_L	Precentral_L	Frontal_Sup_R	Frontal_Inf_Tri_L
Top–29	Cerebelum_7b_L	Supp_Motor_Area_L	Lingual_R	Hippocampus_R

Top	AD vs LMCI		EMCI vs LMCI	
	AD	LMCI	EMCI	EMCI
Top–1	Pallidum_L	Cerebelum_8_L	Putamen_L	Putamen_L
Top–2	Putamen_L	Cerebelum_8_R	Putamen_R	Fusiform_R
Top–3	Cerebelum_8_L	Pallidum_R	Pallidum_R	Pallidum_L
Top–4	Cerebelum_8_R	Putamen_L	Pallidum_L	Putamen_R
Top–5	Putamen_R	Pallidum_L	Temporal_Inf_L	Hippocampus_R
Top–6	Pallidum_R	Putamen_R	Fusiform_L	Pallidum_R
Top–7	Cerebelum_6_L	Hippocampus_R	Fusiform_R	Fusiform_L
Top–8	Cerebelum_7b_R	Vermis_8	Temporal_Inf_R	Hippocampus_L
Top–9	Fusiform_L	Cerebelum_7b_L	Hippocampus_R	Temporal_Inf_R
Top–10	Insula_R	Cerebelum_6_L	Insula_L	Temporal_Inf_L
Top–11	Cerebelum_Crus2_R	Cerebelum_4_5_R	Olfactory_R	Cingulum_Mid_R
Top–12	Vermis_8	Fusiform_R	Rolandic_Oper_R	Thalamus_L
Top–13	Vermis_7	Cingulum_Mid_R	Cerebelum_6_L	Cerebelum_6_L
Top–14	Cerebelum_9_R	Vermis_6	Temporal_Mid_R	Insula_R
Top–15	Lingual_R	Cerebelum_9_R	Insula_R	Cerebelum_4_5_L
Top–16	Cerebelum_6_R	Thalamus_L	Frontal_Inf_Orb_R	Cerebelum_8_L
Top–17	Hippocampus_R	Cerebelum_7b_R	Hippocampus_L	Olfactory_R
Top–18	Fusiform_R	Temporal_Mid_R	Rolandic_Oper_L	Insula_L
Top–19	Cerebelum_4_5_R	Cerebelum_6_R	Cerebelum_7b_R	Cingulum_Mid_L
Top–20	Cerebelum_9_L	Cerebelum_4_5_L	Cerebelum_7b_L	Cerebelum_6_R
Top–21	Cerebelum_7b_L	Vermis_7	Cingulum_Mid_R	Rolandic_Oper_R
Top–22	Insula_L	Cerebelum_Crus2_R	ParaHippo_R	Precentral_L
Top–23	Olfactory_L	Insula_L	Cerebelum_3_R	ParaHippo_R
Top–24	Rolandic_Oper_L	Olfactory_R	Thalamus_R	Cerebelum_4_5_R
Top–25	Olfactory_R	Rectus_L	Thalamus_L	Cerebelum_7b_R
Top–26	Precuneus_L	Temporal_Inf_R	Olfactory_L	Thalamus_R
Top–27	Cerebelum_Crus1_L	Temporal_Mid_L	Cingulum_Mid_L	ParaHippo_L
Top–28	Rolandic_Oper_R	Rolandic_Oper_L	Frontal_Med_Orb_R	Temporal_Mid_R
Top–29	Thalamus_L	Lingual_R	Cerebelum_4_5_R	Amygdala_L

Supplementary Table 2. Top 25% ROIs that show distribution differences between disease group pairs.

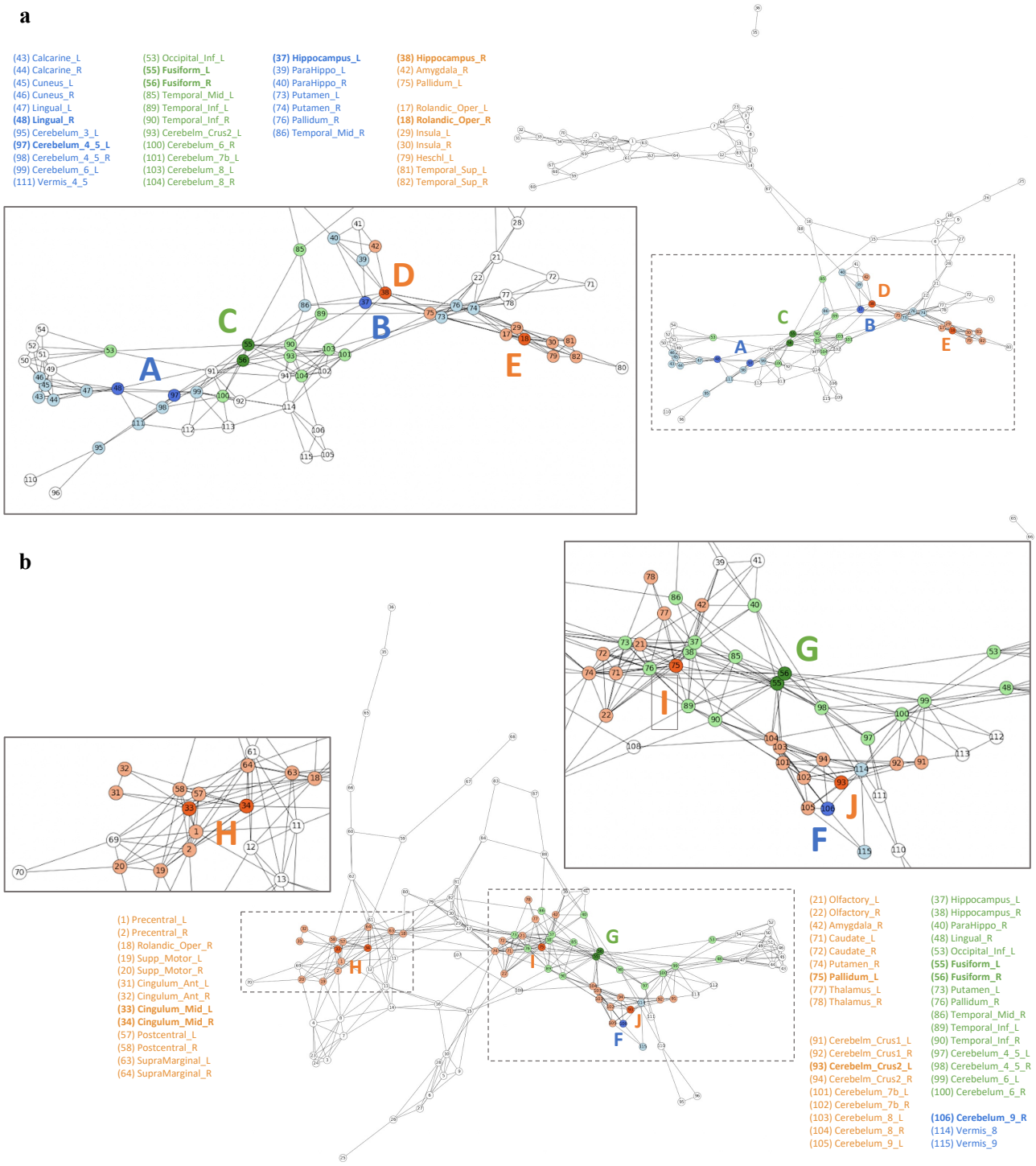

Figure 4. **(a)** AD group summary FCN and **(b)** EMCI group summary FCN. The darker saturation colors indicates meaningful ROIs of each group using LSIRM and ROI nodes which are directly connected to this meaningful ROIs are represented by the same color with a lower brightness level. Here D, E, H, I, and J indicate clusters that exhibit more pronounced responses in the respective group than in the comparative group (orange colored cluster), with C and G representing clusters responsive in both diseases (green colored cluster), while A, B, and F signifies a cluster responsive solely in one group (blue colored cluster).

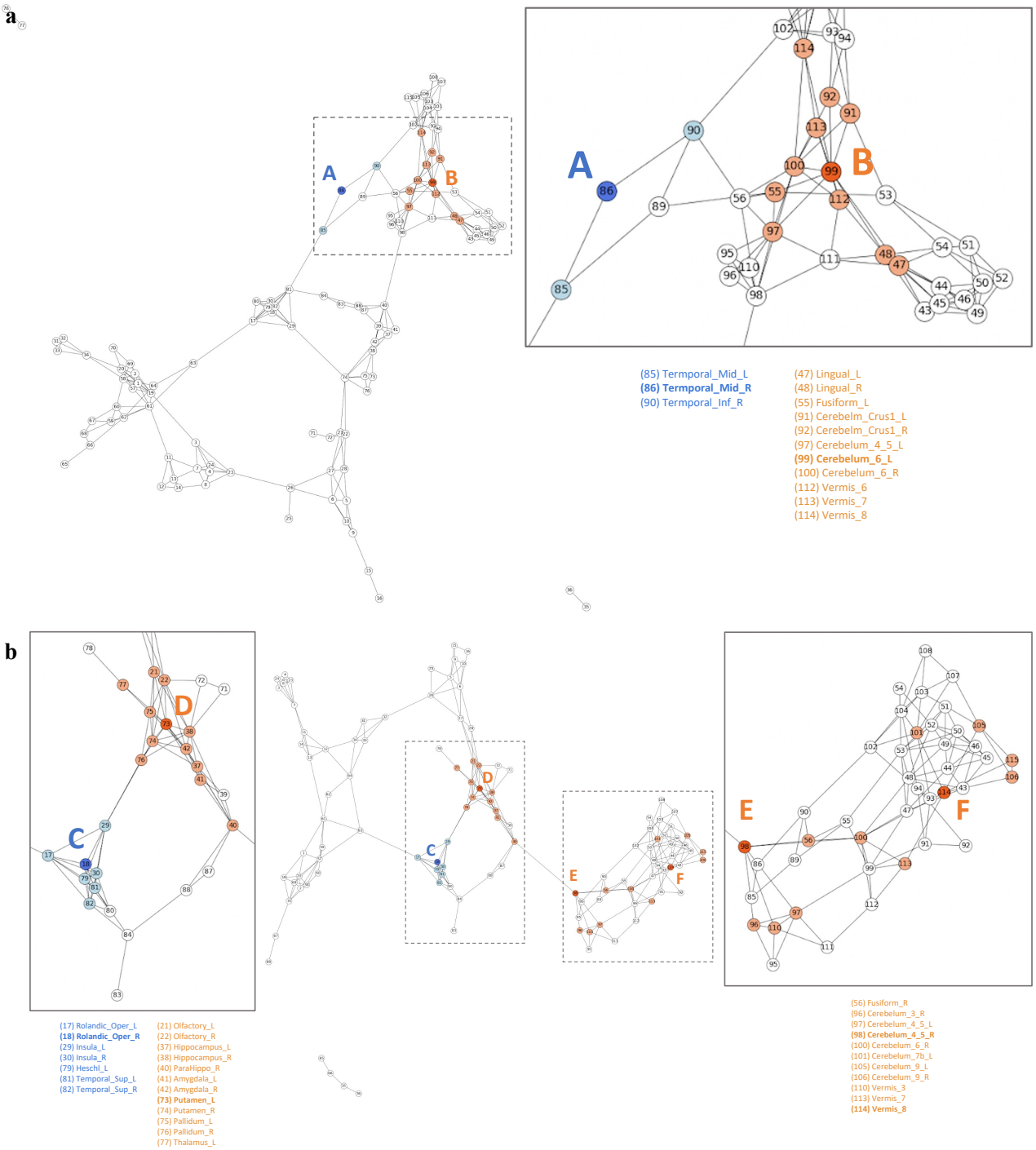

Figure 5. (a) AD group summary FCN and **(b)** LMCI group summary FCN. The darker saturation colors indicates meaningful ROIs of each group using LSIRM and ROI nodes which are directly connected to this meaningful ROIs are represented by the same color with a lower brightness level. Here B, D, E, and F indicate clusters that exhibit more pronounced responses in the respective group than in the comparative group (orange colored cluster), while A and C signifies a cluster responsive solely in one group (blue colored cluster).

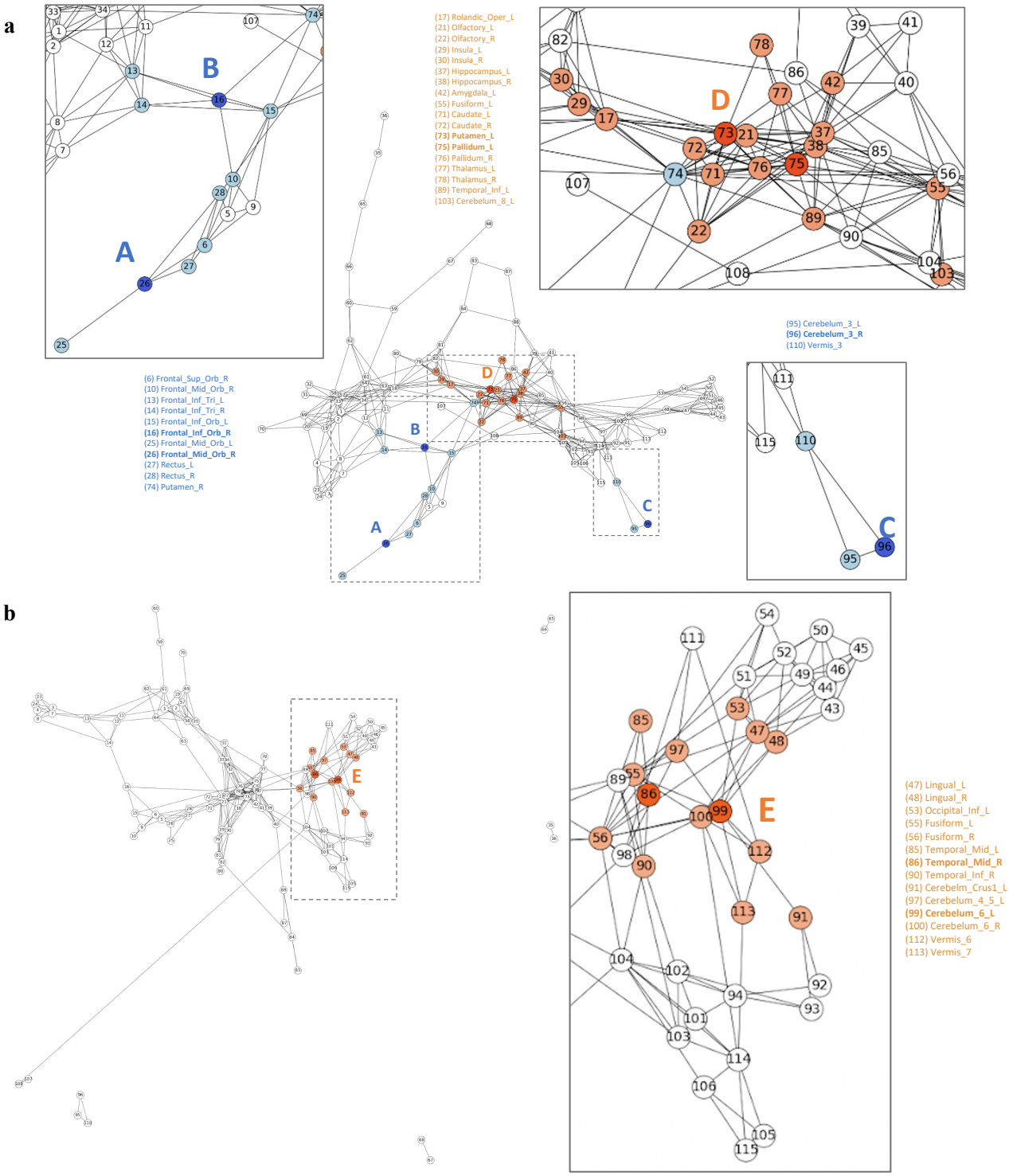

Figure 6. **(a)** EMCI group summary FCN and **(b)** LMCI group summary FCN. The darker saturation colors indicates meaningful ROIs of each group using LSIRM and ROI nodes which are directly connected to this meaningful ROIs are represented by the same color with a lower brightness level. Here the orange colored cluster D and E indicate clusters that exhibit more pronounced responses in the respective group than in the comparative group, while A, B and C signifies a cluster responsive solely in EMCI and not in LMCI.